Mon. Not. R. Astron. Soc. **299,** 637–642 (1998)

Large-scale coherent dipole anisotropy?

S. Basilakos[1,2] and M. Plionis[1]

[1] *National Observatory of Athens, Lofos Nimfon, Thesio, 18110 Athens, Greece*
[2] *Physics Dept, University of Athens, Panepistimiopolis, Greece*

Accepted 1998 March 30. Received 1998 January 29; in original form 1997 October 1

ABSTRACT

We have reanalysed and compared the dipoles of the 1.2-Jy and 0.6-Jy (QDOT) *IRAS* galaxy samples. We find strong indications from both samples for (a) significant contributions to the gravitational field that shapes the Local Group motion from depths up to $\sim 170\,h^{-1}$ Mpc and (b) a large-scale coherence of the dipole anisotropy, indications provided mainly by the fact that the differential dipoles of large equal-volume shells are aligned with the CMB dipole and exhibit significant dipole signals. The two *IRAS* dipoles are indistinguishable within $50\,h^{-1}$ Mpc and beyond $\sim 130\,h^{-1}$ Mpc while the QDOT dipole, having a lower flux limit, continues growing with respect to the 1.2-Jy sample up to $\sim 100\,h^{-1}$ Mpc in agreement with Rowan-Robinson et al.

Key words: galaxies: distances and redshifts – cosmology: observations – large-scale structure of Universe – infrared: galaxies.

1 INTRODUCTION

The peculiar velocity of the Local Group (LG) of galaxies with respect to the cosmic microwave background (CMB), with $u_{\rm LG} = 622\,{\rm km\,s^{-1}}$ towards $(l, b) = (277°, 30°)$, is a well-established fact (cf. Kogut et al. 1993). The most probable cause for this motion as well as for the observed peculiar motions of other galaxies and clusters (cf. Dekel 1997 and references therein) is gravitational instability (cf. Peebles 1980). This is supported by the fact that the gravitational dipole (acceleration) of many different samples of extragalactic mass tracers is well aligned with the general direction of the CMB dipole (cf. Yahil, Walker & Rowan-Robinson 1986; Lahav 1987; Lynden-Bell, Lahav & Burstein 1989; Miyaji & Boldt 1990; Rowan-Robinson et al. 1990; Strauss et al. 1992; Hudson 1993; Scaramella, Vettolani & Zamorani 1991; Plionis & Valdarnini 1991; Branchini & Plionis 1996). However, what still seems to be under discussion is the depths from which density fluctuations contribute to the gravitational field that shapes the Local Group motion. The largest such depth is defined by the dipole *convergence depth*, $R_{\rm conv}$, which is that depth where the true gravitational acceleration converges to its final value. The outcome of many studies, using different flux- or magnitude-limited galaxy samples, is that the apparent value of $R_{\rm conv}$ differs from sample to sample, in the range from 40 to $100\,h^{-1}$ Mpc, with a strong dependence on the characteristic depth of the sample. This probably implies that the apparent dipole convergence is spurious, due to lack of adequate sampling of the distant density fluctuations. Only the optical Abell/ACO cluster sample is volume-limited out to a large enough depth ($\simeq 240\,h^{-1}$ Mpc) to allow a more reliable determination of $R_{\rm conv}$, which was found to be $\simeq 160\,h^{-1}$ Mpc (Scaramella et al. 1991; Plionis & Valdarnini 1991; Branchini & Plionis 1996). Recently, this result has been confirmed using X-ray cluster samples, which are free of the various systematic effects from which the optical catalogues suffer (Plionis & Kolokotronis 1998).

If there is a linear bias relation between the cluster, the galaxy and the underlying matter density fluctuations, as usually assumed (cf. Kaiser 1984), then the galaxy dipole should also have similarly deep contributions. In this study we reanalyse the 1.2-Jy and the deeper QMW–Cambridge–Durham (QDOT) 0.6-Jy *IRAS* galaxy dipoles, initially investigated by Strauss et al. (1992) and Rowan-Robinson et al. (1990) respectively, with the aim of investigating whether there are any such indications.

2 *IRAS* GALAXY SAMPLES AND SELECTION FUNCTIONS

We use in our analysis the two available flux-limited 60-μm *IRAS* samples; one limited at $S_{\rm lim} = 1.2$ Jy (Fisher et al. 1995) and the other at $S_{\rm lim} = 0.6$ Jy (Rowan-Robinson et al. 1990), which has a 1 in 6 sampling rate. The *IRAS* 1.2-Jy sample contains 5763 galaxies with $|b| > 5°$ while the QDOT one contains 2086 galaxies with $|b| > 10°$. Note that although the two catalogues are not totally independent, a cross-correlation revealed only 105 common galaxies (with $\delta\theta \leq 0.^{\circ}6$ and $\delta cz \leq 800\,{\rm km\,s^{-1}}$).

To estimate the local acceleration field it is necessary to recover the true galaxy density field from the observed flux-limited samples. This is done by weighting each galaxy by $\phi^{-1}(r)$, where the selection function, $\phi(r)$, is defined as the fraction of the galaxy number density that is observed above the flux limit at some distance r. Therefore

$$\phi(r) = \frac{1}{\langle n_{\rm g}\rangle}\int_{L_{\rm min}(r)}^{L_{\rm max}} \Phi(L){\rm d}L \qquad (1)$$

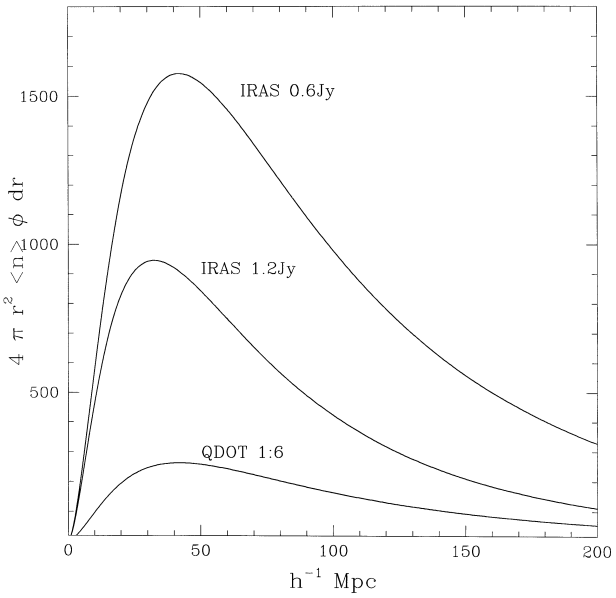

Figure 1. The expected $N(r)$ distribution, according to the *IRAS* galaxy luminosity function, for the 1.2-Jy, the QDOT 0.6-Jy and the PSCz 0.6-Jy *IRAS* samples.

where $L_{\rm min}(r) = 4\pi r^2 \nu S_{\rm lim}$ is the luminosity of a source at distance r corresponding to the flux limit $S_{\rm lim}$, $\nu = 60\,\mu$m and $\langle n_{\rm g}\rangle$ is the mean galaxy number density, given by integrating the luminosity function over the whole luminosity range, with $L_{\rm min} = 7.5\times 10^7\ h^2\,{\rm L}_\odot$ since lower luminosity galaxies are not represented well in the available samples (cf. Rowan-Robinson et al. 1990; Fisher et al. 1995), and $L_{\rm max} = 10^{13}\ h^2\,{\rm L}_\odot$. Obviously, $\phi(r)$ is a decreasing function of distance because a smaller fraction of the luminosity function falls above the flux limit at greater distances.

For the QDOT sample we used the Saunders et al. (1990) luminosity function while for the *IRAS* 1.2-Jy sample we used the parametrized selection function of Yahil et al. (1991). We have verified, however, that the two selection functions are indistinguishable from each other when applied to the same flux limit.

In Fig. 1 we present the $N(r)$ distribution of the *IRAS* 1.2- and 0.6-Jy samples, for the 1-in-6 (QDOT) as well as the unavailable 6-in-6 (PSCz) sampling rate. It is evident that although the QDOT sample is deeper, it samples the galaxy distribution more sparsely than the 1.2-Jy sample.

3 DIPOLE CALCULATION

We determine the peculiar acceleration of Local Group galaxies by measuring moments of the *IRAS* galaxy distribution. The dipole moment, $\boldsymbol{D} = \sum \phi^{-1}(r) r^{-2}\hat{r}$, is calculated by weighting the unit directional vector pointing to the position of each galaxy with the gravitational weight of that galaxy and summing over all available galaxies with distances greater than 5 h^{-1} Mpc (on smaller scales the observed galaxies do not adequately represent the true distribution; cf. Rowan-Robinson et al. 1990). Similarly the monopole term is $M = \sum \phi^{-1}(r) r^{-2}$.

We then estimate the gravitational acceleration induced on the LG from the distribution of *IRAS* galaxies by

$$\boldsymbol{V}_{\rm g}(r) = \frac{H_0 R_{\rm conv}}{M(\leq R_{\rm conv})}\boldsymbol{D}(r) \qquad (2)$$

(cf. Miyaji & Boldt 1990; Plionis, Coles & Catelan 1993). Using linear perturbation theory (cf. Peebles 1980) and equation (2) we can relate the Local Group peculiar velocity to the estimated acceleration by

$$\boldsymbol{u}_{\rm LG}(r) = \beta_{IRAS}\boldsymbol{V}_{\rm g}(r) \qquad (3)$$

where $\beta_{IRAS} = \Omega^{0.6}/b_{IRAS}$ and b_{IRAS} is the *IRAS* galaxy to underlying mass bias factor.

3.1 Treatment of the *IRAS* galaxy data

Owing to systematic effects and biases present in the data we have to perform various corrections, to the raw dipole estimates. First we need to treat the excluded (because of cirrus emission) Galactic plane. We do so by extrapolating to these regions the data from the rest of the unit sphere with the help of a spherical harmonic expansion of the galaxy surface density field and a sharp mask (cf. Yahil et al. 1986; Lahav 1987). Secondly, about 4 per cent of the sky is not covered by the catalogue and we apply to these areas a homogeneous distribution of galaxies having the mean weight estimated from the rest of the sky. Thirdly, due to discreteness effects and the steep selection function with depth we have an additive dipole term, the *shot-noise dipole*, for which we have to correct our raw dipole estimates. Assuming Gaussianity, the Cartesian components of the shot noise dipole are equal ($\sigma_x = \sigma_y = \sigma_z$) and thus $\sigma^2_{\rm 3D} = 3\sigma^2_{i,\rm 1D}$ (cf. Hudson 1993). Taking the coordinate system such that one of the shot-noise dipole components is parallel to the z-axis of the true dipole, we can attempt an approximate correction of the raw dipole according to the following model:

$$D_{\rm cor} = D_{\rm raw} - \sigma_{\rm 3D}/\sqrt{3}. \qquad (4)$$

Note that this correction model, although more severe than the usual $D^2_{\rm cor} = D^2_{\rm raw} - \sigma^2_{\rm 3D}$ model, provides qualitatively similar dipole corrections. We choose, however, to use this model in order to be conservative and to obtain a lower limit to the resulting dipole, as far as the shot-noise correction is concerned, and thus via equation (3) an upper limit to the estimated cosmological β parameter (see Section 4.4).

To calculate $\sigma_{\rm 3D}$ we use two methods; the first is a Monte Carlo simulation approach in which we randomize the angular coordinates of all galaxies while keeping their distance, and thus their selection function, unchanged while the second is the analytic estimation of Strauss et al. (1992): $\sigma^2_{\rm 3D} \simeq \sum \phi_i^{-1} r_i^{-4}(\phi_i^{-1} + 1)$. Fig. 2 shows the difference (in velocity units) between the two shot-noise estimates. It is evident that the two methods give equivalent results, although due to the statistical nature of the first method we believe that it performs better on large depths, where the number density of *IRAS* galaxies is very low.

3.2 z to 3D frame correction

The final but essential correction is to transform redshifts to 3D distances in order to minimize the so called 'Kaiser' effect (Kaiser 1987). This effect can be understood by noting that the distribution of galaxies in redshift space differs from that in real comoving space by a non-linear term:

$$cz = H_0 r + [\boldsymbol{v}(r) - \boldsymbol{v}(0)]\cdot\hat{r}, \qquad (5)$$

where $\boldsymbol{v}(0)(\equiv\boldsymbol{u}_{\rm LG})$ is the peculiar velocity of the Local Group and $\boldsymbol{v}(r)$ the peculiar velocity of a galaxy at position $\boldsymbol{r}$. If $\boldsymbol{v}(r)$ has random orientation, then $\int \boldsymbol{v}(r)\cdot\hat{\boldsymbol{r}}\,{\rm d}^3 r \approx 0$ and the last term of equation (5) is dominated by the LG term; we thus obtain that in

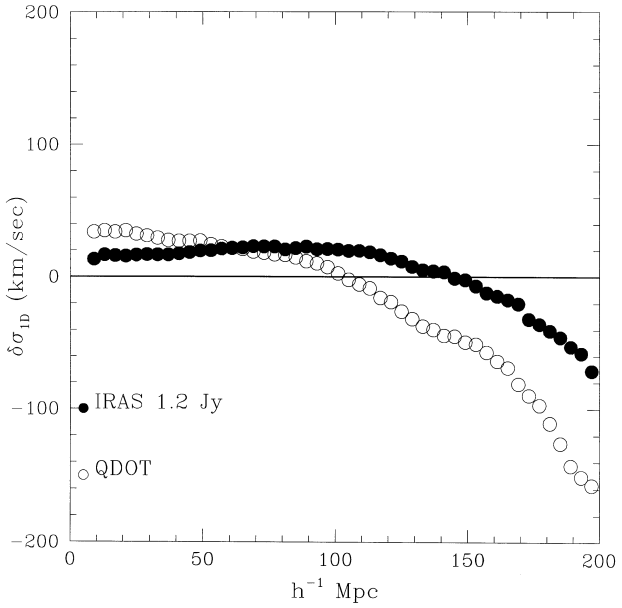

Figure 2. Difference between the Monte Carlo and the Strauss et al. (1992) 1D shot-noise estimates, for both *IRAS* 1.2-Jy and QDOT samples.

the LG frame (i.e. when using $cz = H_0 r$) structures in the direction of our motion appear at a redshift smaller than their true distance in the CMB frame, and thus they will artificially enhance the amplitude of the gravitational dipole.

However, many studies indicate that local galaxies have peculiar velocities not randomly oriented but rather participating in a coherent flow (bulk motion) together with the Local Group [i.e. $\boldsymbol{v}(r) \approx \boldsymbol{v}(0)$] within at least a volume of radius $\sim$5000 km s^{-1} (cf. Lynden-Bell et al. 1988; Dekel 1994, 1997; Strauss & Willick 1995). If so, it would be reasonable to evaluate the *IRAS* dipole in the LG frame, since in this case $cz \approx H_0 r$. However, this is not absolutely true since there should also exist a velocity component due to the local, non-linear dynamics acting between nearby galaxies and/or clusters of galaxies. We can therefore view the galaxy peculiar velocities as consisting of two vector components, a bulk flow and a local non-linear term:

$$\boldsymbol{v}(r) = \boldsymbol{V}_{\rm bulk}(r) + \boldsymbol{v}_{\rm nl}(r). \quad (6)$$

Inserting equation (6) in equation (5) and assuming that $\boldsymbol{v}(r)\cdot\hat{\boldsymbol{r}} \approx \boldsymbol{V}_{\rm bulk}(r)\cdot\hat{\boldsymbol{r}}$, i.e. that the dominant component is that of the bulk flow,[1] we can use the observed bulk flow profile, as a function of distance, given by Dekel (1994, 1997) and combined with that of Branchini, Plionis & Sciama (1996) to correct the galaxy redshifts. The zero-point, $V_{\rm bulk}(0)$, and the direction of the bulk flow are estimated by applying equation (6) at $r = 0$ and assuming, due to the 'coldness' of the local velocity field (cf. Peebles 1988), that $\boldsymbol{v}_{\rm nl}(0) \simeq \boldsymbol{v}_{\rm inf}$ (where $v_{\rm inf}$ is the LG infall velocity to the Virgo Supercluster). Using the average value from the literature, ie. $v_{\rm inf} \simeq 170$ km s^{-1}, we obtain $V_{\rm bulk}(0) \simeq 500$ km s^{-1} towards $(l, b) \simeq (276°, 15°)$.

We test our model by comparing the peculiar velocities that it provides with those resulting from the full dynamical algorithm (kindly provided by Dr Enzo Branchini) which estimates, using linear theory, the gravitational acceleration at the position of each galaxy and then recovers the real-space galaxy distances by solving iteratively the generalized Hubble law of equation (5) (cf. Yahil et al. 1991; Strauss et al. 1992). In Fig. 3 we present this comparison for relatively local galaxies in regions of $\delta\rho/\rho < 1$ (since at dense regions the non-linear component that we neglect in our model will dominate the galaxy peculiar velocity). We find a good correlation within $cz \sim 4000$ km s^{-1}, which is in fact the region where such corrections can affect the dipole. The correlation, at larger distances, progressively fades away since the bulk flow amplitude is low at such distances and the galaxy peculiar velocities are dominated by the distant *local* dynamics. In any case at such distances we do have $\int \boldsymbol{v}(r)\cdot\hat{\boldsymbol{r}}\, {\rm d}^3 r \approx 0$ and thus redshift-space distortions are dominated by the LG term in equation (5) for which we do indeed correct the galaxy redshifts. Note that we have verified that the amount of scatter seen in Fig. 3 is well reproduced from our model if we include a randomly oriented non-linear velocity component with $\langle(\boldsymbol{v}_{\rm nl}\cdot\hat{\boldsymbol{r}})^2\rangle^{1/2} \approx 320$ km s^{-1}.

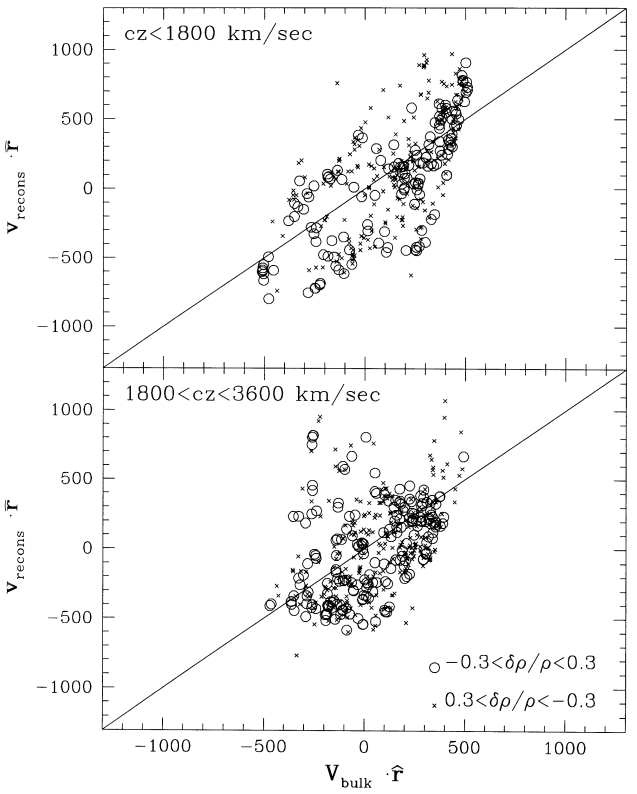

Figure 3. Comparison of local 1.2-Jy *IRAS* galaxy peculiar velocities provided by our model and by the full iterative algorithm within $cz \sim 3600$ km s^{-1} (see text). The diagonal line corresponds to $\boldsymbol{v}_{\rm recons}\cdot\hat{\boldsymbol{r}} = \boldsymbol{V}_{\rm bulk}\cdot\hat{\boldsymbol{r}}$.

We have further tested the robustness of the recovered real-space distribution by performing 200 Monte Carlo simulations in which we vary $v_{\rm inf}$ [and therefore also the amplitude and, slightly, the direction of $\boldsymbol{V}_{\rm bulk}(0)$] as well as the amplitude of $V_{\rm bulk}(r)$ for all rs, by randomly sampling a Gaussian having as mean (μ) the nominal velocity values and $\sigma = 2\mu/3$. Furthermore, we investigate how our results change when using the bulk flow direction of Lauer & Postman (1994); i.e. $(l, b) \simeq (343°, 52°)$ with $|V_{\rm bulk}(r)| = 650$ km s^{-1} for $r \leq 130\, h^{-1}$ Mpc.

Finally, we would like to point out that it so happens that the *IRAS* dipole, estimated in either the LG or the CMB frames, which

[1] In a sense we assume that the vector average of $\boldsymbol{v}_{\rm nl}(r)\cdot\hat{\boldsymbol{r}}$ over a whole-sky distribution of galaxies is $\simeq$0, not an unreasonable assumption in the limit of dense sampling.

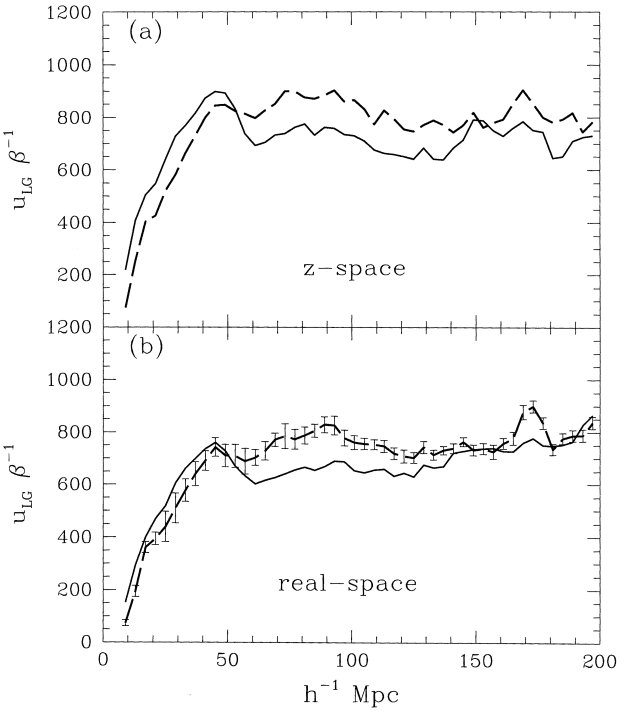

Figure 4. (a) *IRAS* 1.2-Jy (continuous line) and QDOT (dashed line) dipoles in redshift space. (b) The corresponding dipoles in real space. The error bars (shown only for the QDOT dipole) are estimated from Monte Carlo simulations of the velocity field model (see text).

should provide upper and lower dipole bounds respectively, differs very little and thus the z to 3D frame correction *does not have a major consequence in our main dipole results*. We do however investigate, in Section 4.2, possible systematic effects that could be introduced by the frame transformation procedure in our *IRAS*–CMB dipole alignment results.

4 MAIN RESULTS

In Fig. 4(a) we present the two *IRAS* dipoles in redshift space. We observe that they are consistent, although up to $\sim$50 h^{-1} Mpc the 1.2-Jy dipole is systematically higher than the QDOT dipole. However, once we correct for redshift-space distortions (Fig. 4b) the two corrected dipoles almost coincide within 50 h^{-1} Mpc, as they should since both samples, due to their relatively low flux limits, are good tracers of the local Universe. Up to $\sim$130 h^{-1} Mpc the amplitudes of the two real-space dipoles deviate, with the QDOT one being larger than the *IRAS* 1.2-Jy one, which is to be expected since the QDOT sample has a lower flux limit and thus it can 'see' the distant matter fluctuations better than the 1.2-Jy sample. Beyond $\sim$130 h^{-1} Mpc, however, the two *IRAS* dipoles coincide again. As can be seen from Fig. 4, redshift-space distortions enhance the real-space dipole significantly (by $\sim$ 12 per cent) only within $\sim$50 h^{-1} Mpc. The uncertainties of the velocity field model, probed by the Monte Carlo simulations discussed previously, introduce a small scatter in the real-space dipole as indicated by the error bars in Fig. 4(b). Using the Lauer & Postman (1994) bulk flow leaves our main dipole results unaltered with only a small ($\sim$40 km s^{-1}) amplitude decrease.

4.1 Evidence for > 100 h^{-1} Mpc dipole contributions

Between $\sim$150 and 180 h^{-1} Mpc there is an apparent amplitude bump, seen in both redshift and real-space *IRAS* dipoles. This bump is accompanied by a $\sim$5° decrease of the misalignment angle between the two *IRAS* dipoles and that of the CMB, the overall misalignment angles at $r = 200\,h^{-1}$ Mpc being $\sim$23° and $\sim$35° for the 1.2-Jy and QDOT samples, respectively. These facts suggest that this dipole amplitude bump is not due to shot-noise uncertainties but rather it is an intrinsic effect, indicating the existence of contributions to the Local Group motion from such large scales. Such contributions cannot be accurately determined, however, from the present flux-limited samples and deeper samples are required for such a task (see Kolokotronis et al. 1996). To further investigate these probable deep *IRAS* dipole contributions we estimate the differential dipole in large equal-volume shells (see Plionis et al. 1993 for an earlier attempt in z-space). We investigate shell sizes ranging from 2.5×10^6 to $8.2\times10^6\ h^{-3}$ Mpc^3 which give qualitatively similar results. In Tables 1 and 2 we present the differential dipole directions and misalignment angles with respect to the CMB dipole as well as a measure of the significance of the dipole of each individual shell, given by

$$\frac{S}{N}=\frac{D_{\rm raw}}{\sigma_{\rm 3D}}\cos(\delta\theta_{\rm cmb}), \tag{7}$$

for the case of $\delta V \simeq 5.5\times10^6\ h^{-3}$ Mpc^3 (six shells). We observe that for the QDOT sample there are three shells with relatively small misalignment angles and dipole signal-to-noise ratios $S/N > 1$, the deepest shell being [159–175] h^{-1} Mpc, in which $\delta\theta_{\rm cmb} \sim 5°$. For the 1.2-Jy sample, which although shallower has better sampling, we have small misalignment angles ($\delta\theta_{\rm cmb} \lesssim 27°$) in the same shells but also in a deeper shell (188–200 h^{-1} Mpc). Out of these four aligned shells there are significant dipole contributions ($S/N > 1$) only in three, while the probability that these alignments are random is extremely low. The formal probability that two vectors are aligned within $\delta\theta$ is given by the ratio of the solid angle that corresponds to $\delta\theta$ to the solid angle of the whole sphere, i.e. $p_{\rm f}(\delta\theta) = \sin^2(\delta\theta/2)$.

Table 1. Differential 1.2-Jy *IRAS* dipole directions, the corresponding misalignment angles with respect to the CMB dipole, the dipole signal-to-noise ratio and probabilities of alignment within $\delta\theta$ (see text for complete definition). The error bars are estimated from Monte Carlo simulations of the velocity field model, with the last two shells having no corresponding uncertainties because we take $V_{\rm bulk}(r) = 0$ for $r > 170\ h^{-1}$ Mpc (see text).

h^{-1}Mpc	$N_{\rm gal}$	S/N	$l°$	$b°$	$\delta\theta_{\rm cmb}$	$p_{\rm mc}$	$p_{\rm f}$
5-110	4329	4.7±0.2	246.0	35.5	26±3	0.003	0.051
110-139	390	0.6±0.2	311.8	84.1	55±17	0.522	0.213
139-159	220	1.7±0.2	268.9	8.5	22±4	0.026	0.036
159-175	128	0.6±0.2	307.1	31.5	26±7	0.073	0.051
175-188	72	0.0	96.6	61.4	89	0.655	0.492
188-200	59	1.6	282.8	43.2	14	0.029	0.016

Table 2. QDOT dipole results (as in Table 1).

h^{-1}Mpc	$N_{\rm gal}$	S/N	$l°$	$b°$	$\delta\theta_{\rm cmb}$	$p_{\rm mc}$	$p_{\rm f}$
5-110	1267	2.3±0.2	232.5	30.3	38±3	0.016	0.011
110-139	210	−0.1±0.2	98.8	36.6	113±26	0.89	0.71
139-159	96	1.2±0.2	271.1	−12.7	43±9	0.116	0.134
159-175	66	1.2±0.1	272.1	31.6	5±2	0.004	0.002
175-188	53	−0.9	164.4	−73.7	125	0.55	0.78
188-200	31	0.7	318.4	−15.6	60	0.55	0.25

We can now estimate the joint probability of alignment, within the observed $\delta\theta_{\rm cmb}$, of N independent vectors, which is given by

$$P^N \approx \prod_{i=1}^{N} p_i(\delta\theta)/p_i(90^\circ). \quad (8)$$

Between three shells (first, fourth and sixth) the *IRAS* galaxy correlation function is zero, due to the large distances involved, and consequently the shells can be considered to be independent. Due, however, to the vicinity and therefore the possible correlation between the third and fourth QDOT shell, we will consider their joint probabilities as limits. Therefore, we have that the joint probability of alignment between the CMB and the differential *IRAS* equal-volume dipole directions (for those with significant dipole signal $S/N > 1$) is

$$2\times10^{-4} \lesssim P^{2,3}_{\rm QDOT} \lesssim 8\times10^{-4},$$

$$P^{3}_{\rm 1.2Jy} \simeq 2\times10^{-4}$$

for the QDOT and *IRAS* 1.2-Jy samples, respectively.

4.2 Test for systematic alignment errors

The observed differential dipole alignments could in principle be due to errors in the correction used to recover the 3D frame in which we measure the dipole. For example, if redshift errors, especially at large distances where the sampling rate is low, were comparable to a significant fraction of the LG velocity, then using the 3D galaxy distances estimated from equations (5), (6) and $v(0) = 622\ {\rm km\,s^{-1}}$, we could artificially produce a false alignment of the distant-shell differential dipole with that of the CMB. We therefore address the question of which dipole alignments are induced totally due to our frame transformation procedure, i.e. for the extreme case where there is no intrinsic dipole and no LG peculiar velocity. We run 5000 Monte Carlo simulations in which we destroy the intrinsic *IRAS* galaxy dipole as well as redshift-space distortions by randomizing the angular coordinates of the galaxies while keeping their distances and therefore their selection function unchanged. On this intrinsically random galaxy distribution we apply our z to 3D space transformation and then measure the artificially induced differential dipole alignments due to the frame transformation itself. The coupling between the space distortion and the selection function results in a non-trivial alignment behaviour. In the first shell we observe anti-alignments while at more distant shells the artificial alignment effect does appear. For example at the last shell the median $\delta\theta$ is $\sim67^\circ$ instead of 90°. However, it is impossible to create the observed *IRAS* dipole alignments if there is no true signal present. We quantify this by measuring the probability, $p_{\rm mc}(\delta\theta)$, of observing in our Monte Carlo simulations dipole alignments as large as the observed *IRAS* differential dipole alignments. For the shells of interest we find that this probability is low and comparable to the expected $p_{\rm f}$, which implies that the frame transformation uncertainties cannot induce the observed *IRAS* dipole alignments (see the corresponding values of $p_{\rm mc}$ and $p_{\rm f}$ in the tables).

We conclude that the differential dipole directions are not randomly oriented with respect to the CMB and therefore we have indications not only for significant dipole contributions from large depths but also for a coherent anisotropy extending to these large scales.

4.3 Possible cause of the large-scale *IRAS* dipole contributions

It is interesting that stronge evidence exists for deep dipole contributions from the available galaxy cluster data. Contributions up to $\sim$20–30 per cent of the total cumulative optical and X-ray cluster dipole were found from $\sim$140–160 h^{-1} Mpc depths (Scaramella et al. 1991; Plionis & Valdarnini 1991; Branchini & Plionis 1996; Plionis & Kolokotronis 1998). Similar *coherence* of the differential dipoles in equal-volume shells was also found in galaxy cluster samples (Plionis & Valdarnini 1991; Plionis et al. 1993). These studies have shown that the cause of the deep dipole contributions should be attributed mostly to the Shapley concentration, a huge mass overdensity located at $\sim140\ h^{-1}$ Mpc in the general direction of the Hydra–Centaurus supercluster (Shapley 1930; Scaramella et al. 1989; Raychaudhury 1989).

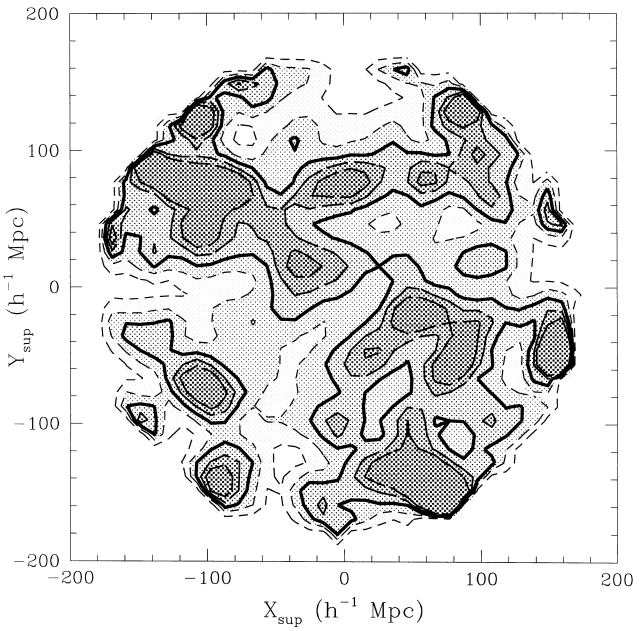

Figure 5. Contour plot of the smoothed 1.2-Jy *IRAS* galaxy distribution in real space and on the supergalactic plane.

To investigate further the possible cause of the present *IRAS* dipole results we have smoothed the *IRAS* 1.2-Jy galaxy distribution in a 40^3 cube with a cell size of $10\ h^{-1}$ Mpc using a Gaussian with smoothing radius equal to one cell and weighting each galaxy by ϕ^{-1}. Due to the coupling between the selection function and the constant-radius smoothing, we correct the resulting smoothed distribution for a distance-dependent effect, which we quantified using N-body simulations (details will be presented in a forthcoming paper). In Fig. 5 we present the smoothed *IRAS* 1.2-Jy galaxy distribution on the supergalactic plane (of $10\ h^{-1}$ Mpc width) within $170\ h^{-1}$ Mpc. The contour step is 0.4 in overdensity while the $\delta\rho/\rho = 0$ level appears as a thick continuous line.

Well-known structures appear in this plot; the largest and most evident are the Shapley concentration located at $(X_{\rm sup}, Y_{\rm sup})\approx(-120, 60)$, the Perseus–Pisces supercluster at $(X_{\rm sup}, Y_{\rm sup})\approx(60, -40)$, the Coma supercluster at $(X_{\rm sup}, Y_{\rm sup})\approx(-20, 70)$, the Ursa Major supercluster at $(X_{\rm sup}, Y_{\rm sup})\approx(100, 100)$ and the Pisces–Cetus supercluster at $(X_{\rm sup}, Y_{\rm sup})\approx(50, -140)$, while the Great Attractor (Hydra–Centaurus complex?), at $(X_{\rm sup}, Y_{\rm sup})\approx(-30, 30)$ appears in the foreground of the Shapley concentration. Furthermore, Fig. 5 is very similar to the corresponding Abell/ACO cluster density field (cf. Tully et al. 1992; Branchini & Plionis 1996, their fig. 3), and we therefore obtain a consistent picture, from both *IRAS* galaxy and Abell/ACO cluster data, in which the Shapley concentration is the most probable cause of

the deep dipole contributions while the general alignment of the Great Attractor, Perseus–Pisces and Shapley superclusters is most probably the cause of the apparent *coherence* of the *IRAS* galaxy dipole.

4.4 $\Omega_0^{0.6}/b_{IRAS}$ from the *IRAS* dipoles

Using the real-space dipole results and equation (3), we can estimate the density parameter β_{IRAS}. However, the value obtained should be considered an upper limit since the deep contributions to the dipole, for which we do have strong indications, are probably not fully revealed by the present samples (see Kolokotronis et al. 1996). Taking into account the scatter among the two *IRAS* samples, the amplitude variations at large depths and the uncertainties of the velocity model used to recover the real-space galaxy distances, we find

$$\beta_{IRAS} \lesssim 0.78(\pm 0.1), \tag{9}$$

in agreement with the QDOT analysis of Rowan-Robinson et al. (1990) but slightly larger, although within 1σ, than the 1.2-Jy results of Strauss et al. (1992). This value of β_{IRAS} implies either that $\Omega_0 \lesssim 0.66$ for $b_{IRAS} = 1$ or $\Omega_0 \simeq 1$ for $b_{IRAS} \gtrsim 1.28$.

5 CONCLUSIONS

Using a consistent analysis procedure we find that within $50\ h^{-1}$ Mpc both the 1.2-Jy and 0.6-Jy (QDOT) *IRAS* samples give identical dipole results, while beyond this depth the QDOT dipole increases substantially up to $100\ h^{-1}$ Mpc, in agreement with Rowan-Robinson et al. (1990). Furthermore there are significant indications for (a) dipole contributions from depths $\sim 170\ h^{-1}$ Mpc, in agreement with other recent large-scale studies (cf. Plionis & Kolokotronis 1998) and (b) a coherence of the dipole anisotropy extending to similar depths. The most probable cause of these deep dipole contributions is the Shapley mass concentration, while the most probable cause of the dipole *coherence* is the general alignment, on the supergalactic plane, of the Perseus–Pisces supercluster, the Great Attractor and the Shapley concentration, which span a range of $\sim 200\ h^{-1}$ Mpc.

A similar study of the complete (6 in 6) *IRAS* 0.6-Jy sample (PSCz) should give better indications of these results, although the overall amplitude of the effect could probably be estimated by a deeper catalogue (limited at a lower flux limit).

ACKNOWLEDGMENTS

We thank Enzo Branchini for providing us with the reconstructed *IRAS* 1.2-Jy galaxy peculiar velocities. SB thanks the Greek State Fellowship Foundation for financial support (Contract No 2669).

REFERENCES

Branchini E., Plionis M., 1996, ApJ, 460, 569
Branchini E., Plionis M., Sciama D. W., 1996, ApJ, 461, L17
Dekel A., 1994, ARA&A, 32, 371
Dekel A., 1997, in da Costa L., ed., Galaxy Scaling Relations: Origins, Evolution & Applications. Springer, in press
Fisher K. B., Huchra J. P., Strauss M. A., Davis M., Yahil A., Schlegel D., 1995, ApJS, 100, 69
Hudson M. J., 1993, MNRAS, 265, 72
Kaiser N., 1984, ApJ, 284, L9
Kaiser N., 1987, MNRAS, 227, 1
Kogut A. et al., 1993, ApJ, 419, 1
Kolokotronis V., Plionis M., Coles P., Borgani S., Moscardini L., 1996, MNRAS, 280, 186
Lahav O., 1987, MNRAS, 225, 213
Lauer T. R., Postman M., 1994, ApJ, 425, 418
Lynden-Bell D., Faber S. M., Burstein D., Davies R. L., Dressler A., Terlevich R. J., Wegner G., 1988, ApJ, 326, 19
Lynden-Bell D., Lahav O., Burstein D., 1989, MNRAS, 241, 325
Miyaji T., Boldt E., 1990, ApJ, 353, L3
Peebles P. J. E., 1980, The Large Scale Structure of the Universe. Princeton Univ. Press, Princeton NJ
Peebles P. J. E., 1988, ApJ, 332, 17
Plionis M., Kolokotronis V., 1998, ApJ, 500, 1
Plionis M., Valdarnini R., 1991, MNRAS, 249, 46
Plionis M., Coles P., Catelan P., 1993, MNRAS, 262, 465
Raychaudhury S., 1990, Nat, 342, 251
Rowan-Robinson M. et al., 1990, MNRAS, 247, 1
Saunders W., Rowan-Robinson M., Lawrence A., Efstathiou G., Kaiser N., Ellis R. S., Frenk C. S., 1990, MNRAS, 242, 318
Scaramella R., Baiesi-Pillastrini G., Chincarini G., Vettolani G., Zamorani G., 1989, Nat, 338, 562
Scaramella R., Vettolani G., Zamorani G., 1991, ApJ, 376, L1
Shapley H., 1930, Harvard Obs. Bull., 874, 9
Strauss M. A., Willick J. A., 1995, Phys. Rep., 261, 271
Strauss M. A., Yahil A., Davis M., Huchra J. P., Fisher K., 1992, ApJ, 397, 395
Tully R. B., Scaramella R., Vettolani G., Zamorani G., 1992, ApJ, 388, 9
Yahil A., Walker D., Rowan-Robinson M., 1986, ApJ, 301, L1
Yahil A., Strauss M., Davis M., Huchra J. P., 1991, ApJ, 372, 380

This paper has been typeset from a $\TeX$/$\LaTeX$ file prepared by the author.